ELSEVIER

Contents lists available at ScienceDirect

Atmospheric Research

journal homepage: www.elsevier.com/locate/atmosres



A numerical study on the ventilation coefficients of falling lobed hailstones

Pao K. Wang^{a,b,*}, Chih-Che Chueh^a

- ^a Research Center for Environmental Changes, Academia Sinica, Taipei, Taiwan
- ^b Department of Atmospheric and Oceanic Sciences, University of Wisconsin, Madison, WI 53706, USA



Keywords:
Ventilation coefficient
Lobed hailstones
High Reynolds numbers
Turbulent flow
Downburst

ABSTRACT

The ventilation coefficients that characterize the enhancement of heat/mass transfer rate due to the falling motion of lobed hailstones created by a set of mathematical expressions in an atmosphere of pressure 460 hPa and temperature 248 K are computed by numerically solving the convective-diffusion water vapor transport equation while the local airflow velocities are obtained through the numerical solution of unsteady Navier-Stokes Equation around the falling hailstones. The atmospheric condition is chosen so that the hailstone is not growing wet and the ventilation coefficient represents dry hailstone condition. The diameters of the hailstones investigated here are 1, 3, 5, 7 and 10 cm with the Reynolds numbers ranging from 9560 to 388,000 respectively. The ventilation coefficients for all cases are nearly the same when the diameter is 1 cm. The difference becomes greater as the size increases. The highest ventilation coefficient calculated here is > 500 for a 10 cm hailstone with 36 long lobes. We found that in general lobed hailstones have larger ventilation effect than spherical hailstones of the same size. We also report that the connection between basic geometry information (i.e. surface area and volume) and the ventilation coefficients. The larger surface area usually results in greater ventilation coefficient whereas no clear relation exists between the ventilation coefficient and volume for the stones investigated here. Empirical formulas for ventilation coefficient as a function of hailstone diameter and Schmidt numbers are given. Implications of these ventilation coefficients are discussed.

1. Introduction

Large hailstones that fall during some violent storms can cause serious damages to crops and properties, even the loss of human lives (e.g., Chou et al., 2013). There have been studies of hail suppression techniques attempting to mitigate such damages but at present reliable technologies to suppress large hail formation in storms are still beyond reach. Large hailstorms can produce strong downbursts and the even more serious microbursts, both thought to be due to very rapid evaporative cooling effect of large hydrometeors including hail, that can also incur severe damages (Fujita, 1985).

For both basic scientific purpose or for developing technologies to mitigate hail damage, the first step should be to understand quantitatively the hailstorm formation process. On the qualitative side, it is generally accepted that hail grows almost exclusively by accreting supercooled water drops in clouds (Knight and Knight, 2005). It is the quantitative side that our knowledge is relatively poor due to difficulties in obtaining some key parameters of hail growth with sufficient accuracy. One of the key parameters is the fall motion of the hailstones and the associated ventilation effect.

The fall motion of hydrometeors in clouds have great impact on their cloud physical properties and one of the most important is the growth rate of these particles as it determined whether the cloud will grow further or dissipate and how fast precipitation can develop. The growth of a hydrometeor generally consists of two major growth modes: (1) collision growth caused by the collision and subsequent coalescence of two or more particles and (2) diffusion growth due to the diffusion of water vapor towards the surface of a hydrometeor when the environment is supersaturated (Wang, 2013). Note that the evaporation process of a hydrometeor is just the reverse diffusion process in which the vapor diffusion is directed outward from the hydrometeor surface. The present paper will focus on the diffusion mode.

The diffusion growth or evaporation rate of hydrometeors depends on the water vapor gradient around it and this gradient is strongly influenced by the flow field around the falling hydrometeor. The vapor density gradient is enhanced in the upstream side of the hydrometeor and relaxed in the downstream side compared with that of a stationary hydrometeor. When averaged over the whole hydrometeor surface, there is always a net enhancement of the vapor gradient. The enhancement factor is called the *ventilation coefficient*. Physically, this

E-mail address: pwang1@wisc.edu (P.K. Wang).

^{*} Corresponding author.

implies that when a hydrometeor is falling in a supersaturated (subsaturated) air, it will grow (evaporate) faster than a stationary one by this factor

A number of previous publications have addressed some relevant experimental and computational issues associated with the ventilation coefficient of falling hydrometeors. For example, Kinzer and Gunn (1951) experimentally measured such coefficients for large water drops. Thorpe and Mason (1966) determined experimentally the ventilation coefficients for falling hexagonal ice crystals. Beard and Pruppacher (1971) conducted laboratory experiments to measure the ventilation coefficients for small evaporating water droplets falling in air using a vertical wind tunnel, Maslivah and Epstein (1970), Woo and Hamielec (1971), and Pitter et al. (1974) were among the first to perform numerical calculations of ventilation coefficient using small water droplets and the oblate spheroids (to represent plate ice crystals). Later, Ji and Wang (1990) numerically computed the ventilation coefficients for falling ice crystals using more realistic shapes of ice columns, hexagonal plates, and broad branch ice crystals. But these studies were concerned with small hydrometeors.

So far there are only a few studies of ventilation coefficients for large ice particles in general and for hailstones in particular. List (1963) studied the general heat and mass transfer during the accretion growth of large hailstones. Macklin (1963) measured the heat transfer rate of melting ice spheres and spheroids of diameter or long axis of 3.8 and 5.1 cm. In List and Dussault (1967), quasi steady state equations and results of calculations of icing and melting conditions as well as the heat and mass exchange of spherical and spheroidal hailstones are investigated covering the whole range of height of a model cloud, showing that the transfer conditions are functions only of the height above the ground level and local content of water substance, and the major diameter of the hailstones. Bailey and Macklin (1968) reported similar experiments for spheroids with diameters of 3-7.2 cm. One can derive the ventilation coefficient from these heat transfer rates, even though they are confined to the accretion growth or melting mode of hailstone. Goyer et al. (1969) measured the rate of heat transfer during melting of solid ice spheres and freezing of spongy ice spheres experimentally, indicating that there is probably time for smaller spongy hailstones to freeze before reaching the ground, but that freezing of spongy hailstones 3 cm in diameter is improbably. Having the experiments carried out in a liquid tunnel where the electrolyte is forced past the stationary particles at variable flow rates under several levels of turbulence intensity, Scheupp and List (1969) made an extrapolation of the results to the heat and mass transfer coefficients of hailstone models in the atmosphere, showing that surface roughness may account for increases in the transfer rates of up to a factor of 2. Prodi et al. (1991) in an experimental study showed that the surface roughness due to the lobes alters the flow field around the hailstone and therefore has significant impact on the ventilation coefficient that cannot be ignored and may be crucial to a representative model. Tlisov et al. (1992) carried out theoretical and experimental studies to establish relationships between the main variables such as the Nusselt number, Sherwood number, Reynolds number, and so on for heat and mass transfer of drops and growth and melting of freely falling hailstones. Measuring the surface temperature distributions of initially warm spherical and spheroidal hailstone models cooling in a wind tunnel experimentally using infrared measurements, the effects of particle shape, rotational motion pattern and Reynolds number on area-specific heat transfer are discussed in Zheng and List (1994), and determination of the heat and mass transfer coefficients was made in Greenman and List (1995). Aguirre Varela et al. (2003) studied experimentally the ventilation effect of regularly uniform surface lobes by measuring their heat transfer rates for Reynolds number range $2000 < N_{Re} < 20,000$, but they restricted themselves to considering only 2D lobed ice cylinders and thus the results may not be applicable to real falling lobed hailstones. Letting a flow past a sphere, Duan et al. (2015) gave a new insight into the traditional experiment, trying to establish a new relationship between



Fig. 1. A hailstone sample collected by PKW on April 13, 2006 in Madison, Wisconsin, showing some lobed examples.

the drag coefficient and the heat transfer. Chouippe et al. (2019) performed the direct numerical simulations with emphasis on the different settling regimes of an ice sphere in an ambient fluid for heat and mass transfer, helping establish the parametrization with four physical parameters including particle to fluid density ratio, Galileo number, Prandtl number, and Richardson number.

The experimental data are highly useful but are limited in size range and confined to the surface conditions. There is a need to determine the ventilation coefficients of the hailstones more systematically and valid for broader atmospheric conditions, and this can be achieved by performing numerical simulations of falling hailstones. Thus, Cheng et al. (2014) conducted a numerical study on the ventilation coefficients around the falling hailstones, assuming that the hailstones are spherical in shape. Such an assumption is normally justifiable as Matson and Huggins (1980) found that 84% of the hailstones they observed in free fall were spheroidal. Yet, it is also known that hailstones have different levels of surface irregularity due to surface roughness and often forming lobed shapes and Fig. 1 shows such an example. The hailstones in this figure are about 3–5 cm in diameter and only mildly lobed. There are large hailstones that are strongly lobed and highly irregular shaped (e.g., Knight and Knight, 2005) but the concentration is likely small.

In this study, we present the results of numerical calculations of the ventilation coefficients of falling lobed hailstones of shape created by the mathematical expressions proposed in our previous work (see Wang et al., 2015). The present paper is organized as follows. In Section 2, the mathematical models for ventilation coefficient determination, the governing equations, and the mathematical expressions used to generate the lobed hailstones are presented, followed by the results and discussions in Section 3 and future outlooks in the final section.

2. Physics and mathematics

2.1. Ventilation coefficient determination

The water vapor flux density around a falling hailstone surface can be expressed as

$$\overrightarrow{j_{v}} = -D_{v} \nabla \rho_{v} + \rho_{v} \overrightarrow{u}, \tag{1}$$

where D_{ν} is the diffusivity of water vapor in air and is considered a constant in the present work, and ρ_{ν} is the water vapor density. The air velocity \overrightarrow{u} is obtained by numerically solving the Navier-Stokes equation of the hailstone falling in air. The flux expression (1) can be combined with the continuity equation (see Wang, 2013) to obtain the unsteady convective diffusion transport equation for water vapor:

$$\frac{\partial \rho_{\nu}}{\partial t} = -\nabla \cdot \overrightarrow{j}_{\nu} = D_{\nu} \nabla^{2} \rho_{\nu} - \overrightarrow{u} \cdot \nabla \rho_{\nu}. \tag{2}$$

Note that after we take the divergence of Eq. (1), $\nabla \cdot (\overrightarrow{u} \rho_{\nu})$ is reduced to $\overrightarrow{u} \cdot \nabla \rho_{\nu}$ under the incompressible assumption $\nabla \cdot \overrightarrow{u} = 0$. Once ρ_{ν} is obtained by solving Eq. (2), the hailstone diffusion growth rate that is given by the total flux of water vapor towards the hailstone surface can be calculated through:

$$\left(\frac{dm}{dt}\right) = -\oint_{S} (D_{\nu} \nabla \rho_{\nu})_{surface} \cdot d\vec{S}, \qquad (3)$$

where $d\overrightarrow{S}$ stands for the increment of the hailstone surface. The minus sign before the surface integral indicates that the inward flux is calculated (because it is the inward flux that results in growth). The ventilation coefficient is then determined by

$$\overline{f}_{\nu} = \frac{(dm/dt)}{(dm/dt)_0},\tag{4}$$

where $(dm/dt)_0$ represents the growth rate of a stationary hailstone. The term $\overline{f_v}$ is the mean ventilation coefficient (called ventilation coefficient hereafter) for vapor diffusion that is the subject of this paper.

Following the previous work for a spherical hailstone by Cheng et al. (2014), we assume that the water vapor is saturated at hailstone surface and the hailstone is falling in an air having a supersaturation of 2%; that is, the relative humidity at the surface of the hailstone is 100% whereas that far away from the hailstone is 102%. In terms of vapor density, the boundary conditions are therefore

$$\rho_v = 5.5257 \times 10^{-4} kg \cdot m^{-3} \quad at \quad r = a$$
 (5)

$$\rho_v = 5.6362 \times 10^{-4} kg \cdot m^{-3} \quad at \quad r \to \infty \ .$$
 (6)

Note that the ventilation coefficient depends only on the flow field and its value does not depend on the degree of saturation. Thus our assumption of a 102% saturation ratio in the far field is set just so that numerical calculations can proceed. Otherwise it is just as good as any other saturation degree assumed.

The numerical procedure is to first solve the Navier-Stokes equation for the falling hailstone to obtain the velocity field that is then used in Eq. (2) to get the vapor density distribution. We used the computational fluid dynamic package Fluent 15.0 of ANSYS, Inc., as the solver and selected the numerical scheme Quadratic Upstream Interpolation for Convective Kinematics (QUICK) to solve the Navier-Stokes equation with the incompressible condition. The Navier-Stokes equation and the boundary conditions for solving the flow field are:

$$\frac{\partial \overrightarrow{u}}{\partial t} + (\overrightarrow{u} \cdot \nabla) \overrightarrow{u} = -\frac{\nabla p}{\rho_a} + \nu \nabla^2 \overrightarrow{u} + \overrightarrow{g}$$
(7)

$$\nabla \cdot \overrightarrow{u} = 0 \tag{8}$$

where \vec{u} is the air velocity, p the static pressure, ρ_a air density, the kinematic viscosity of air and \vec{g} the gravity. The boundary conditions are:

$$\vec{u} = 0$$
 at the hailstone surface, (9)

$$\vec{u} = u_{\infty} \cdot \hat{e}_{z}$$
 far away from the hailstone (10)

where u_{∞} is the fall speed of the hail (assumed to be its terminal fall velocity) and \hat{e}_z is the unit normalized vector in the z direction.

2.2. Mathematical expressions and geometry information for lobed hailstones

In Wang et al. (2015), a set of mathematical equations based on successive modification of simple shapes (SMOSS) (Wang, 1997, 1999) was used to describe the shapes of lobed hailstones quantitatively. In the present study, we will use the same set of expressions to represent the shape of the lobed hailstones for the calculation of ventilation

coefficients. The main equation in spherical coordinates is (adopted from Eq. (5) of Wang (1997) with changes of symbols and using cosine instead of sine function):

$$R = p[1 - \cos^2(qw)]^r [1 - \cos^2(ql)]^r + s \tag{11}$$

where R represents the value of the radial coordinate. It is seen from Eq. (11) that R=s when p=0, i.e., it represents a sphere. Thus Eq. (11) generates the shape of a lobed hailstone by adding "protrusions" given by the first term on the right hand side to a sphere of radius s. The x, y and z coordinates of the lobed hailstone surface are given by:

$$x = \cos(w)\cos(l)\{p[1-\cos^2(qw)]^r[1-\cos^2(ql)]^r + s\}$$
 (12)

$$y = \sin(w)\cos(l)\{p[1 - \cos^2(qw)]^r[1 - \cos^2(ql)]^r + s\}$$
 (13)

and

$$z = \sin(l) \{ p[1 - \cos^2(qw)]^r [1 - \cos^2(ql)]^r + s \}, \text{ respectively.}$$
 (14)

The parameter w varies from 0 to 2π and l from -0.5π to 0.5π , respectively. Parameter q controls the number of protrusions. The rest of the parameters (i.e. p, r and s) can be adjusted to produce finer details of the shape and size of the lobed hailstones. The values of these parameters used in the present study are given in Table 1. Further information on how to adjust these parameters to change the shape of the hailstone can be seen in Wang et al. (2015).

Lobed hailstones have different surface areas and volumes, depending on the length and number of protrusions, and these geometric characteristics are important to their heat and mass transfer properties. Since we will compare these transfer rates with that of spherical hailstones, it is useful to examine the ratio of surface area and mass/volume of lobed hailstone to that of an *equivalent sphere*. To enforce a uniform definition across all cases, we define an equivalent sphere as a sphere with diameter the same as the dimension of the lobed hailstone at the equator calculated using Eq. (11). The results of the ratios are shown in Figs. 2 and 3.

Fig. 2 indicates that the surface areas of all the lobed hailstones considered here are greater than that of a corresponding equivalent spherical hailstone, obviously due to their many protrusions. Furthermore, all of the long lobed cases have greater surface areas than their respective short lobed counterparts which is evidently due to their longer lobes. Fig. 3 shows the volume ratio of the lobed hailstones to an equivalent sphere. It is seen that, with the unique exception of 2uv-long case, all other lobed hailstones have volume smaller than that of an equivalent sphere with the ratio ranges from slightly < 0.8 (6uv-long case) to nearly 1 (2uv-short case). This is due to the many voids between the protrusions that reduce the total volume. The exception case of 2uv-long lobed hailstone is partially due to our definition of the equivalent sphere and also partially due to the fact that its shape deviates substantially from a sphere and the additional length of the lobes makes its volume larger than its equivalent sphere.

While it is relatively easy to understand qualitatively why the surface area and volume of these hailstones are different, it is not so simple to quantify the differences systematically due to their complex geometry. This difficulty is quite common in many areas of atmospheric sciences that involve with complex shapes and two well-known examples are the studies of ice particles and aerosol particles. Clearly, it is desirable to find good methods to resolve this difficulty satisfactorily in the future.

Table 1
The parameters used in the set of mathematical expressions (9), (10) and (11).

	Long spiky	Short spiky
p r s	0.5 1 2	1 2 8
5	2	0

Surface Area Ratio

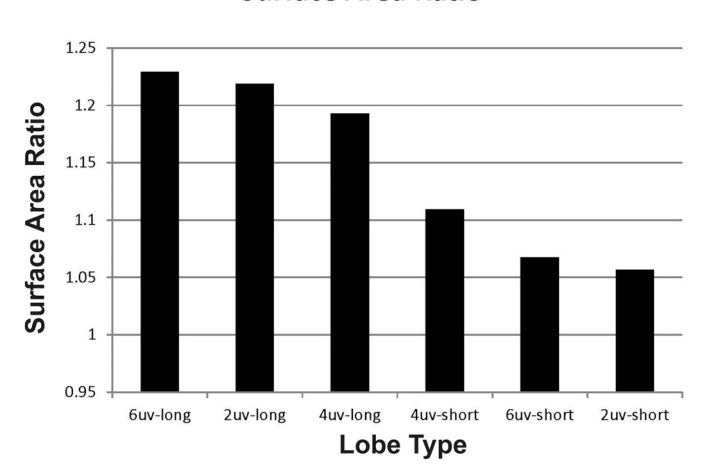


Fig. 2. Surface area ratio (lobed to spherical) of hailstones as a function of lobe type.

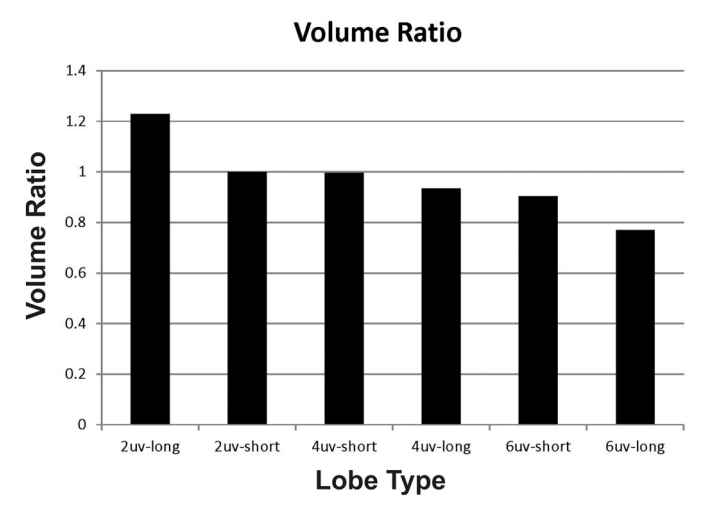


Fig. 3. Volume ratio (lobed to spherical) of hailstones as a function of lobe type.

3. Results and discussions

For this study, we performed calculations to determine the ventilation coefficients for the lobed hailstones of diameters 1, 5, and 10 cm falling in air at $P=460\,\mathrm{hPa}$ and $T=248\,\mathrm{K}$. Under such an environment, the presence of liquid water in a convective cloud in mid-latitudes is very small (Noh et al., 2012), and it is reasonable to assume that the lobed hailstone surface is dry. We set this atmospheric condition so that the computed ventilation coefficient represents the value for dry hailstones. This is exactly the same atmospheric condition assumed by Cheng et al. (2014) in their study of the ventilation effect of falling spherical hailstones, so the results of the present study can be compared directly with theirs.

Wang et al. (2015) conducted numerical calculations of the flow fields around falling lobed hailstones of the same sizes but under a different atmospheric condition (900 hPa and 283 K). The flow characteristics are very similar for similar Reynolds number range. Readers are referred to that paper for details of the solution methods and the characteristics of the flow fields. In the present paper, we will focus on the discussions on the calculated results of ventilation coefficients. Note that the ventilation coefficient is a function of the Reynolds number of the falling particle only (assuming the shape remains the same). The coefficient would stay the same as long as the Reynolds number remains the same for this particle even if the atmospheric condition is different.

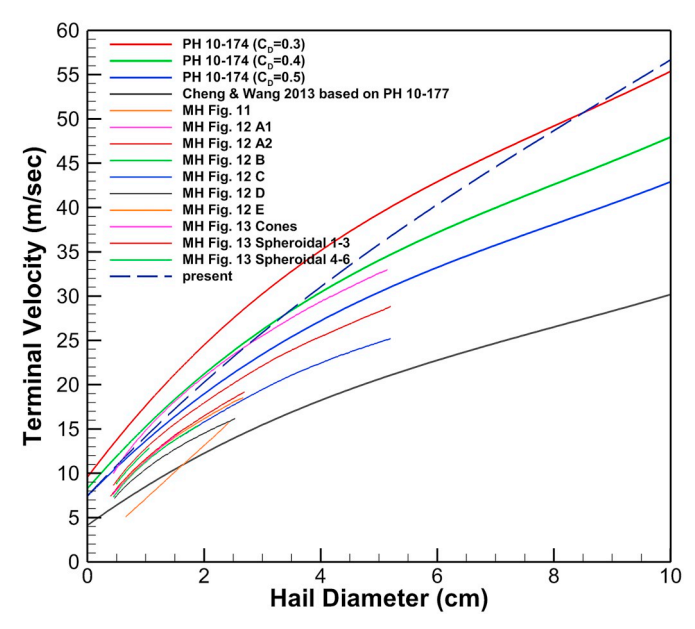


Fig. 4. Terminal velocity versus hailstone diameter. PH and MH refer to Pruppacher and Klett (1997) and Matson and Huggins (1980), respectively. The number following PH represent the equation number in the book. The number following MH stands for the number of Figure used in the reference. MH Fig. 12 A1 curve is for smooth sphere at C_D equal to 0.45 and MH Fig. 12 A2 for 0.6. MH Fig. 12 B curve is taken from Lozowski and Beattie (1979), MH Fig. 12 C from Roos and Carte (1973), MH Fig. 12D from Matson and Huggins (1980), and MH Fig. 12 E from Auer et al. (1971).

The terminal velocities of the lobed hailstones are determined by using an expression given in Pruppacher and Klett (1997) for a quasi-spherical hailstone:

$$u_{\infty} = 0.36 \left(\frac{\rho_H d}{C_D \rho_a}\right)^{0.5},\tag{15}$$

where ρ_H is the density of the hailstone, ρ_a air density, d the diameter of the in cm, and C_D the drag coefficient. The air density for the atmospheric condition considered here is 1.2922×10^{-3} g cm⁻³ and hail density is assumed to be 0.9167 g cm⁻³. In the present study, the values of C_D of hailstones of different sizes are obtained from the average of the drag coefficients of Wang et al. (2015).

The resulting terminal velocities used in the present study are shown in Fig. 4. While the terminal velocities of the same particle size are almost all greater than those of Matson and Huggins (1980), they approach those of Bilham and Relf (1937) and Heymsfield and Wright (2014) under the consideration of ρ_H more or $< 0.9 \, \mathrm{g \, cm^{-3}}$.

The Reynolds number of the hailstone is defined as

$$N_{\rm Re} = \frac{du_{\infty}}{\nu} \tag{16}$$

where ν is the kinematic viscosity of air.

Table 2 shows the values of the diameter, terminal velocity, and Reynolds number of the 1, 3, 5, 7 and 10 cm diameter hailstones

Table 2Dimension, Reynolds number and terminal velocity of the hails whose flow fields are calculated in this study.

Diameter (cm)	New terminal velocity (m/s)	New Reynolds number
1	13.97	9.561E+03
3	25.96	5.330E + 04
5	35.80	1.225E + 05
7	44.67	2.140E + 05
10	56.65	3.876E + 05

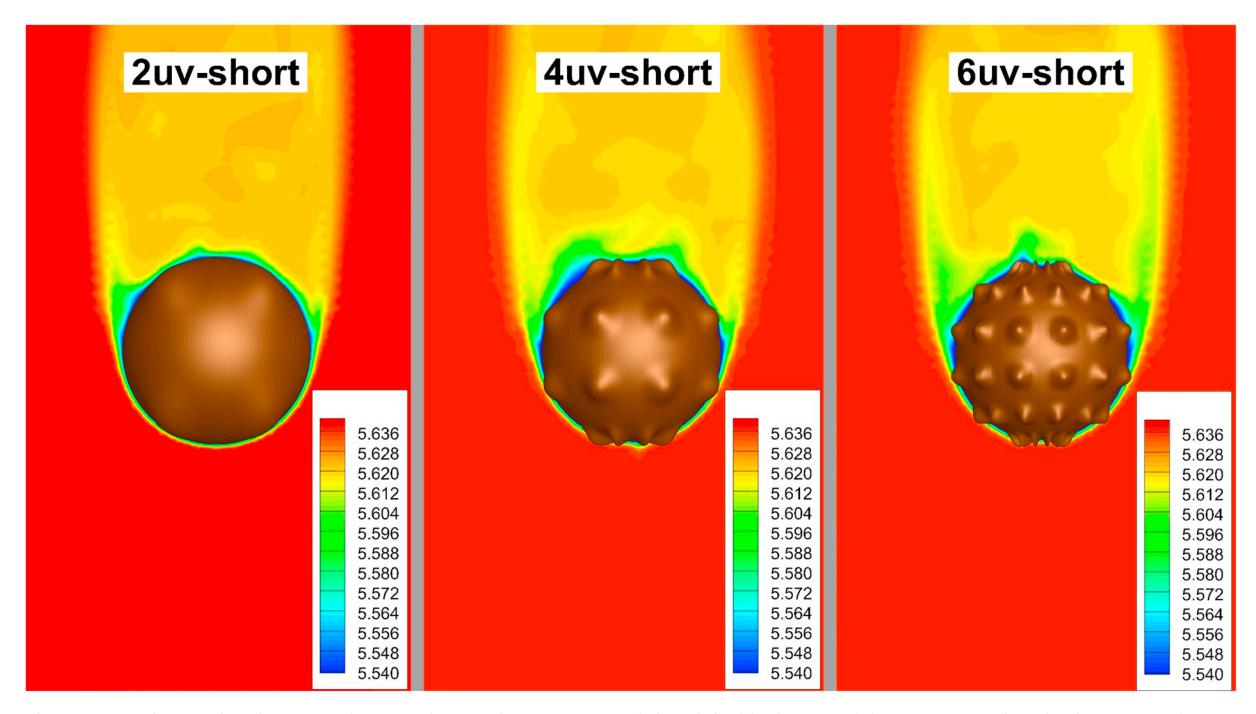


Fig. 5. Vapor density distribution in the central vertical cross-section of short-lobed hailstones of d = 1 cm at randomely chosen time frames.

investigated here.

In the following, we will examine the calculated vapor density distributions and ventilation coefficients for the 6 cases of lobed hailstones. As we shall see, the irregularities on the surface complicate the ventilation behavior greatly so that the ventilation effect is not simply a matter of size or velocity or the number of lobes.

3.1. Short lobed cases

Fig. 5 shows the computed vapor density distribution in the central cross- section of the yz-plane around the three cases of short lobed hailstones of 1 cm diameter. All the front (upstream) sides of the three lobed hailstones are surrounded by high vapor densities, while low vapor densities surround their rear sides, implying that the convective flux $\rho_{\nu} \vec{u}$ is generally dominant over the diffusion flux $-D_{\nu} \nabla \rho_{\nu}$ due to the motion of the hailstones (i.e. the fluid inertial effect on the vapor transport is much greater than the diffusion of water vapor effect.) such that the vapor convective flux $\rho_{\nu} \vec{u}$ in the front points towards the hailstone surface, whereas the flux in the rear is directed away from the surface, which is consistent with the results of spherical hailstones by Cheng et al. (2014).

In general, there is no much difference among these three short lobed hailstones in terms of water vapor distribution (see Fig. 5). The distribution in the front side of the 3 cases are similar, whereas that in the rear show more differences. The drier regions (green color) in the rear near the hailstone surface are somewhat larger and more irregular with increasing number of lobes. This should indicate the formation of more turbulent wakes with increasing number of lobes which prevents higher vapor content air to get close to the hail surface easily.

To further understand the diffusion growth of the lobbed hailstone, we plot the vapor gradient magnitude $|\nabla \rho_{\nu}|$ as shown by Fig. 6.

It is seen here that in all three cases the front side is characterized by high vapor gradient (red color) near the surface while the rear side is low vapor gradient, as they should be. Among the three, however, the 2uv-short case has a nearly hemispherical coverage of high gradient in the front side whereas the coverage becomes smaller and smaller as the number of lobes increase. In the rear side, the 2uv-short case shows three isolated pockets of high gradient areas whereas the number of such pockets also becomes fewer as the number of lobes increases. A

look into the microstructure of the flow field near the rear surface of the hailstone (not shown) reveals that the 2uv-short case has the largest and most organized inflow regions that bring in water vapor towards the surface whereas these inflow regions are smaller and most disorganized for the 6uv-short case. Thus it appears that the irregularities or roughness on the surface hinders the flux of water vapor towards the hailstone. Similar conclusion has been given by Aguirre Varela et al. (2003) who studies similar process for graupel and found that the rear area with turbulent wakes has less heat/mass extraction than the front area. But, at the same time, we note that the surface areas of the 4uv-and 6uv- cases are greater that the 2uv case, so that the increase in area compensates the smaller gradient that results in the very similar ventilation coefficients (under the assumption that all three have the same Reynolds number) as we shall see later.

Fig. 7 shows a randomly chosen frame of the vapor density distribution in the central yz-plane for the case of 5 cm diameter hailstone falling in air. Here we again see that the dry area (the yellow region) in the rear of the hailstone is most extensive in the case of 6uv-short and the thinnest in the 2uv-short case. Thus, one would expect that the vapor flux density towards the surface is the weakest for the 6uv-short case. This is confirmed by Fig. 8, which shows the vapor density gradient around the hailstones where the high gradient areas (red) appears to be the smallest in the 6uv-short case.

Fig. 9 shows the calculated ventilation coefficients $\overline{f_{\nu}}$ of the short lobed hailstones of diameters 1, 3, 5, 7 and 10 cm. It is seen that the relation of $\overline{f_{\nu}}$ versus d is not very simple. For d smaller than \sim 7 cm, $\overline{f_{\nu}}$ of 4uv- and 6uv-short cases are similar and smaller than that of the 2uv-short cases. For d>7 cm, $\overline{f_{\nu}}$ of 4uv- and 6uv-short cases become slightly greater than that of the 2uv-short cases. Apparently, for smaller short-lobed hailstones, the number of lobes seems to hinder the vapor transport towards the surface despite that the surface areas of the 4uv and 6uv cases are greater. On the other hand, for large stones the opposite is true. The exact reason requires more study to clarify. It is possible that the larger size causes the convective transport (the ρ_{ν} \overrightarrow{u} term in Eq. (1)) to increase, and the integration of increased $\nabla \rho_{\nu}$ over the slightly larger surface areas of the 4uv and 6uv stones results in larger $\overline{f_{\nu}}$.

Fig. 9 also shows the $\overline{f_v}$ of spherical hailstones calculated by Cheng et al. (2014). First of all, we note that the $\overline{f_v}$ of the 2uv case is, except for

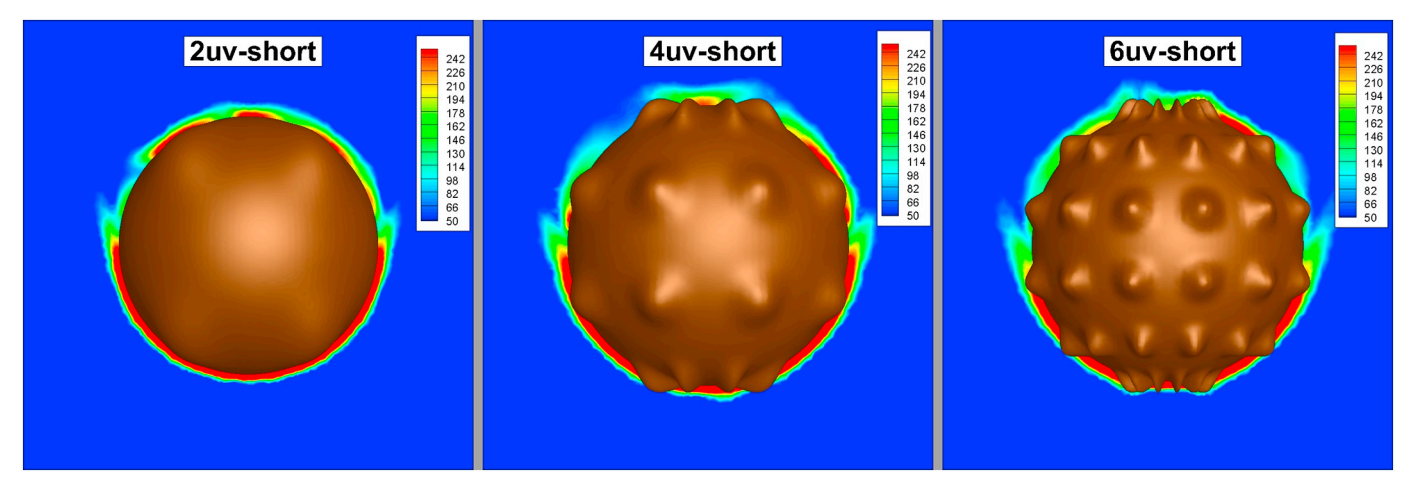


Fig. 6. Vapor density gradient distribution in the central vertical cross-section of short-lobed hailstones of d = 1 cm at time frames corresponding to that in Fig. 5.

d=1 cm, greater than that of a sphere of the same d. For 4uv and 6uv cases, the $\overline{f_{\nu}}$ is smaller than that of a sphere of the same diameter if d<5 cm and becomes larger if d>5 cm. It is seen that for larger hailstones, the lobes help to significantly enhance the ventilation effect.

The curves in Fig. 9 can be fitted by the following empirical expressions:

$$\overline{f_v} = 20.66d - 2.259$$
 for sphere (17)

$$\overline{f_v} = 0.3086d^3 - 3.827d^2 + 47.86d - 34.29$$
 2uv-short (18)

$$\overline{f_v} = 3.687d^2 + 3.713d - 3.569$$
 4uv-short (19)

$$\overline{f_v} = 3.589d^2 + 5.42d - 4.416$$
 6uv-short (20)

Sometimes it is desirable to see the relation between the ventilation coefficient and the Reynolds number instead of the diameter d. Fig. 10 shows this relation using $\log_{10}N_{\rm Re}$ as the parameter.

The fitting equations for curves using $Y = \log_{10} N_{\rm Re}$ in Fig. 10 are as follows:

$$\overline{f}_{v} = \exp(6.867Y - 6.545)$$
 for sphere (21)

$$\overline{f_v} = \exp(9.783Y - 10.92)$$
 2uv-short (22)

$$\overline{f_y} = 151.9Y^3 - 1914Y^2 + 8025Y - 11190$$
 4uv-short (23)

$$\overline{f_v} = 151.9Y^3 - 1914Y^2 + 8025Y - 11190$$
 6uv-short (24)

Eqs. (23) and (24) are identical because the two curves are nearly on top of each other and the polynomial fits of $\bar{f}_{\nu}(Y)$ for the two cases yield the same coefficients.

Another parameter that is often used to characterize the ventilation effect is a dimensionless number defined as $X = (N_{Sc})^{1/3}(N_{Re})^{1/2}$ where N_{Sc} is the Schmidt number defined by $N_{Sc} = \nu/D_{\nu}$ and D_{ν} is the diffusivity of water vapor in air (Pruppacher and Klett, 1997; Wang, 2013). Fig. 11 shows the plot of $\overline{f_{\nu}}$ versus X:

The empirical fit relations including an empirical relation suggested by Rasmussen and Heymsfield (1987) are:

$$\overline{f_{\nu}} = 0.0003137X^2 + 0.386X - 6.483$$
 sphere (25)

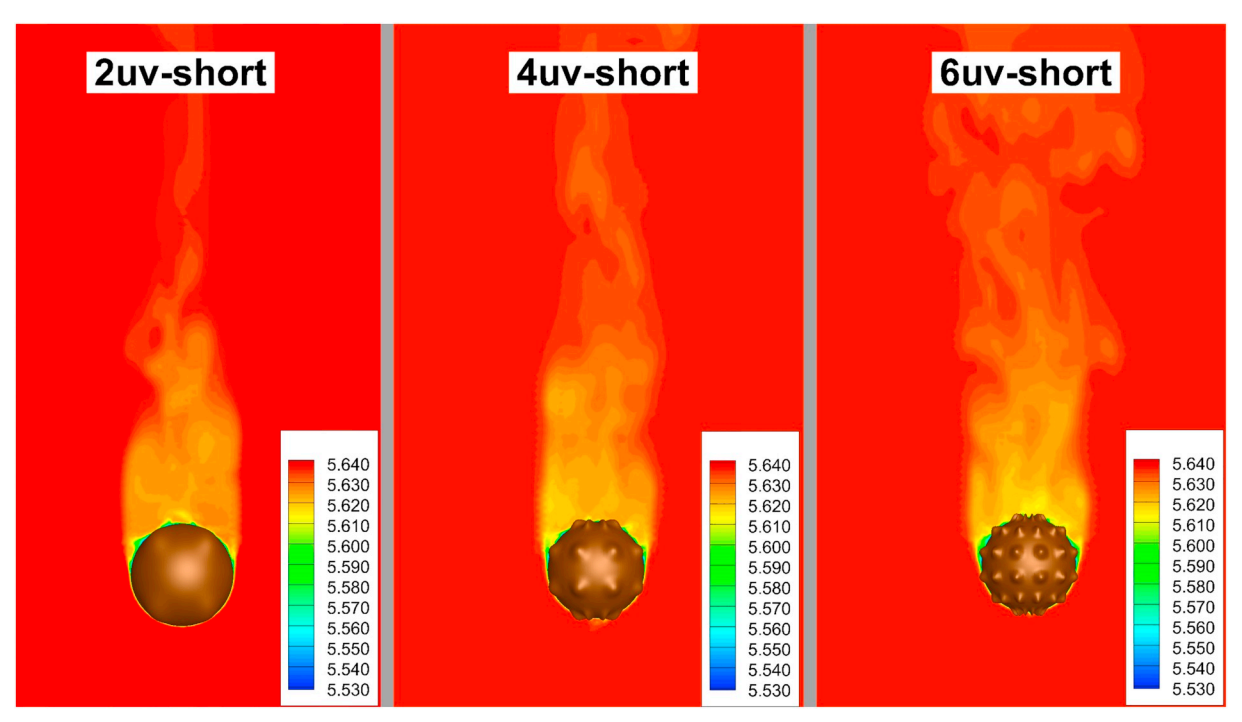


Fig. 7. Vapor density distribution in the central verical cross-section of short-lobed hailstones of d = 5 cm at randomely chosen time frames.

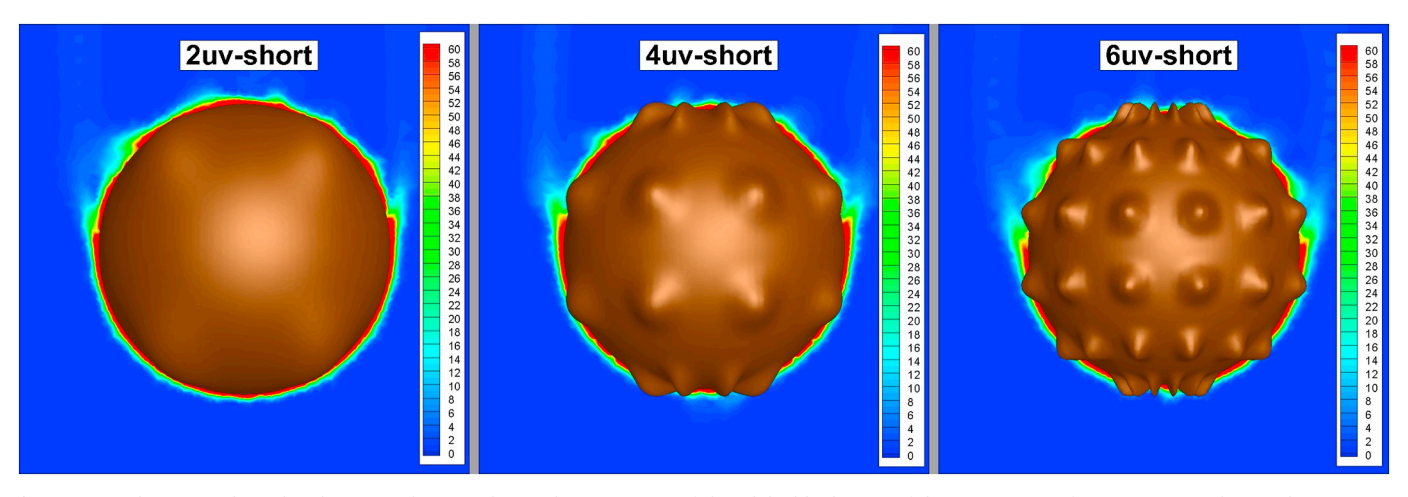


Fig. 8. Vapor density gradient distribution in the central verical cross-section of short-lobed hailstones of $d=5\,\mathrm{cm}$ at time frames corresponding to that in Fig. 7.

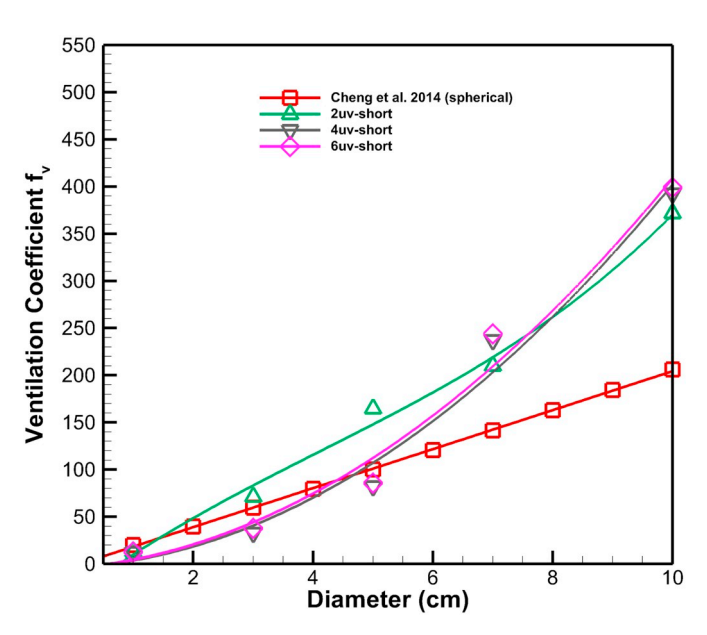


Fig. 9. Ventilation coefficient versus diameter for short lobed and spherical hailstones.

$$\overline{f_v} = 0.00124X^2 + 0.4229X - 18.38$$
 2uv-short (26)

$$\overline{f}_{v} = 0.003014X^2 - 0.2994X + 13.19$$
 4uv-short (27)

$$\overline{f_v} = 0.002953X^2 - 0.2538X + 11.13$$
 6uv-short (28)

$$\overline{f}_v = 0.78 + 0.308X$$
 (Rasmussen and Heymsfield 1987) (29)

Fig. 11 shows that the estimate of ventilation effect may differ greatly if different fit equations in Eqs. (25)–(29) are adopted in cloud models, especially for severe storms when very large hailstones are produced. For storm cases involving only small hailstones (d < 3 cm) the differences would be small.

3.2. Long lobed cases

The results of the long lobed hailstones are shown in this section and we can make a comparison between these hailstones and the short ones present in the previous section. Fig. 12 shows the randomly selected

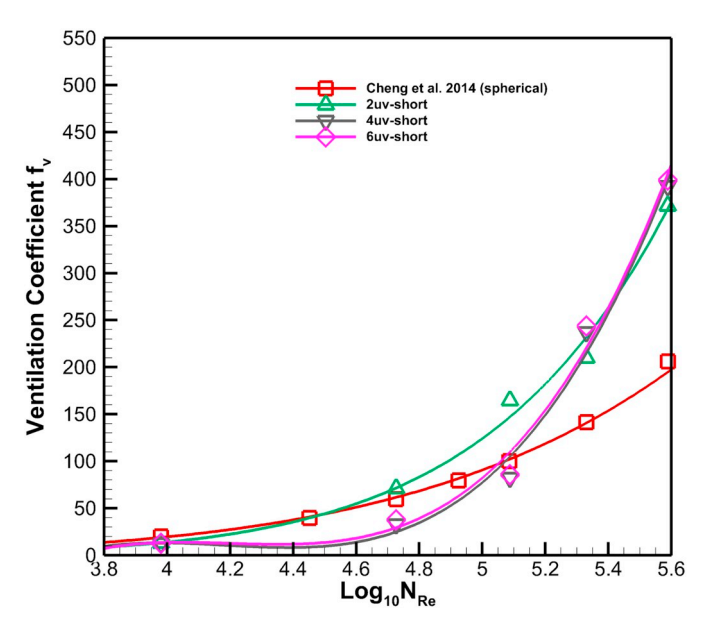


Fig. 10. Ventilation coefficient versus $\log_{10}N_{\rm Re}$ for short lobed and spherical hailstones.

vapor distribution of 1 cm three long lobed cases.

It is seen in this figure that the drier (green) region is generally larger than those of the short lobed cases shown in Fig. 5. Hence it appears that the downstream dry region tends to become greater as the lobe becomes longer. On the other hand, the dry region doesn't always become greater as the number of protrusions rises, since the size of the 4uv green region is smaller than those of the other cases and the 6uv green region appears to be smaller than that of the 2uv case. The situation is complicated undoubtedly due to the complex shape and the exact reason requires further study.

Fig. 13 shows the vapor gradient magnitude distribution of 1 cm long lobed hailstones. Compared with those of the corresponding short lobed cases shown in the previous section, the high gradient areas become smaller due to the presence of more turbulent regions between the long lobes that hinder the fluid flow onto the surface. In addition, as the number of protrusions increases, the high gradient region becomes smaller as it becomes harder for water vapor to enter the spherical part of the hailstone.

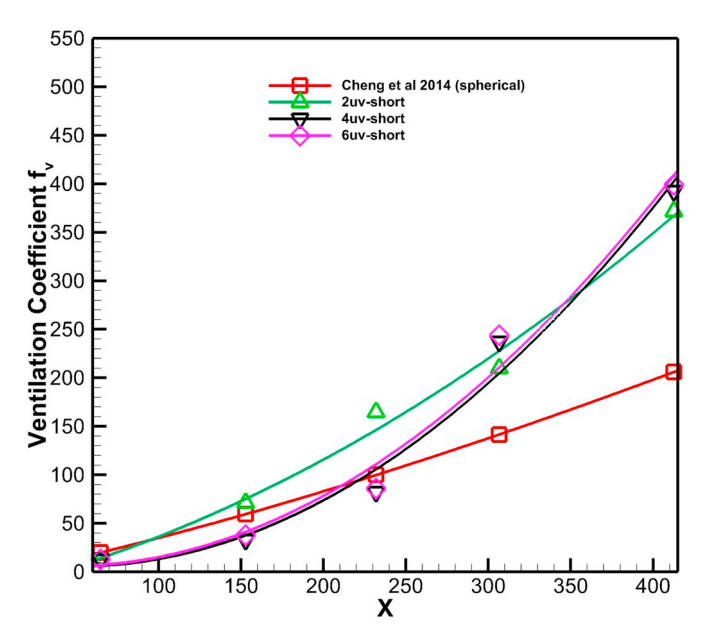


Fig. 11. Ventilation coefficient versus \boldsymbol{X} for short lobed and spherical hailstones.

Figs. 14 and 15 show the water vapor and vapor gradient distributions of 5 cm long lobed hailstones respectively. Again, as in the case of short lobed 5 cm cases in Figs. 7 and 8, the larger hailstone falls faster and the convective vapor flux is strong enough to dominate over the diffusion vapor flux. The high vapor density region now can get closer to spherical surface than does the corresponding short-lobed one. It is also clear that as the hailstone becomes larger and falls faster, the boundary layer becomes thinner permitting the higher density vapor to get closer to the surface.

Fig. 16 shows the calculated ventilation coefficients for long lobed hailstones. For smaller hailstones with d < 3 cm the ventilation coefficients of three cases are close and are only slightly greater than the spherical case. For d > 3 cm, all lobed hailstones have much higher ventilation coefficients than the spherical ones, ranging from \sim 1.5 for d = 4 cm to \sim 2.5 times for d = 10 cm. The three long-lobed curves can be fitted by the following equations:

$$\overline{f_y} = 0.2819d^3 - 3.543d^2 + 49.63d - 37.33$$
 2uv-long (30)

$$\overline{f_y} = -0.5187d^3 + 10.3d^2 - 7.439d + 10.94$$
 4uv-long (31)

$$\overline{f_y} = -0.3016d^3 + 7.277d^2 + 9.418d - 1.024$$
 6uv-long (32)

Fig. 17 shows the ventilation coefficients versus Reynolds number for long-lobed hailstones, and Eqs. (33)–(35) show the corresponding curve fittings:

$$\overline{f}_{v} = \exp(10.08Y - 11.36)$$
 2uv-long (33)

$$\overline{f}_{v} = \exp(10.61Y - 12.15)$$
 4uv-long (34)

$$\overline{f_v} = \exp(10.34Y - 11.56)$$
 6uv-long (35)

Again $Y = \log_{10} N_{Re}$ in Eqs. (32)–(34).

Fig. 18 shows the ventilation coefficients versus the non-dimensional *X* for long-lobed hailstones, and Eqs. (36)–(38) show the corresponding curve fittings:

$$\overline{f_{\nu}} = 4.103 \times 10^{-6} X^3 - 1.778 \times 10^{-3} X^2 + 1.106 X - 55.64$$
 2uv-long (36)

$$\overline{f_{\nu}} = -8.221 \times 10^{-6} X^3 + 7.648 \times 10^{-3} X^2 - 0.7469 X + 31.79$$
 4uv-long (37)

$$\overline{f_{\nu}} = -4.589 \times 10^{-6} X^3 + 5.47 \times 10^{-3} X^2 - 0.2463 X + 9.533$$
 6uv-long (38)

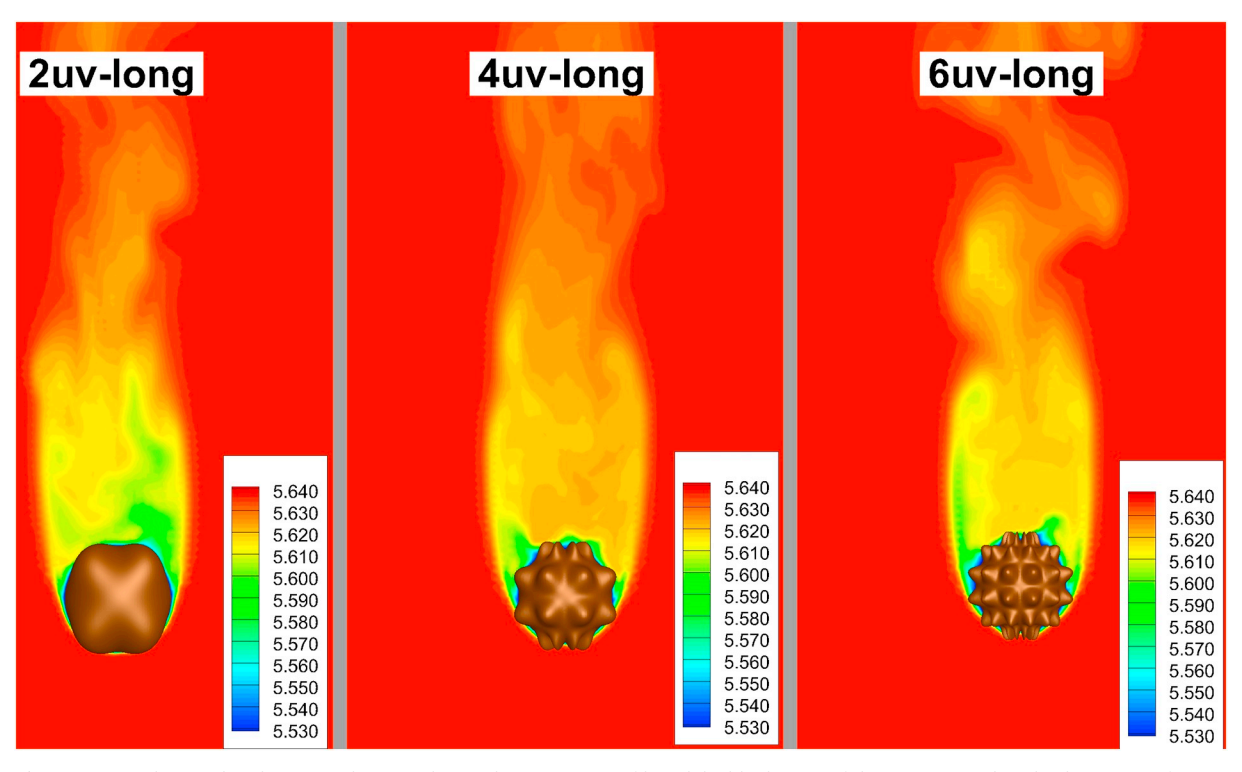


Fig. 12. Vapor density distribution in the central vertical cross-section of long-lobed hailstones of d = 1 cm at randomely chosen time frames.

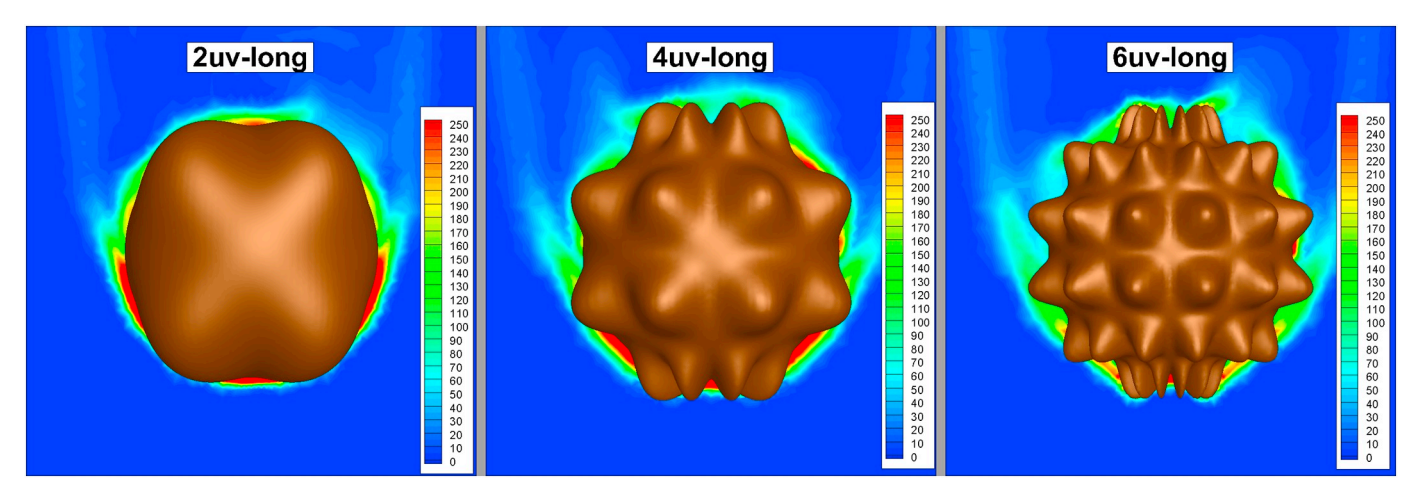


Fig. 13. Vapor density gradient distribution in the central verical cross-section of short-lobed hailstones of d = 1 cm corresponding to the time frames in Fig. 12.

Although the $\bar{f_y}$ reported above is evaluated in terms of water vapor diffusion, it is usually assumed that the ventilation coefficient for heat diffusion $\bar{f_h}$ is the same as $\bar{f_y}$ (Pruppacher and Klett, 1997).

In the above discussions, we presented the ventilation coefficients as a function of d, $N_{\rm Re}$, or X for different kinds of simulated lobed hailstones. While this is useful for understanding the impact of different lobes on ventilation effect, most cloud models probably do not need, or cannot afford, to use ventilation coefficients based on such detailed categorization of lobed hailstones. Rather, an overall assessment of the impact of lobes on ventilation is probably sufficient. Thus, in the following we provide an overall assessment of ventilation effect of falling lobed hailstones ignoring the details.

Fig. 19 plots the ventilation coefficient versus diameter for all hailstones considered here without discriminating the differences of the lobes and then does the curve fitting. This yields the following relationship:

$$\overline{f_{\nu}} = \exp(1.513\log_{10}d + 2.515) \tag{39}$$

where d is in cm.

Similar to Fig. 19, Fig. 20 plots ventilation coefficients versus the surface area for all lobed hailstones and the curve can be fitted by:

$$\overline{f_v} = \exp(0.7586\log_{10}A + 1.54) \tag{40}$$

where A is the surface area (in cm²) of the hailstone.

Fig. 21 does the same except versus volume and the curve can be fitted by:

$$\overline{f_{\nu}} = \exp(0.5142\log_{10}V + 2.823) \tag{41}$$

where V is the volume (in cm³) of the hailstone.

All the above three charts show substantial data spread which is undoubtedly due to the different lobe number and shape.

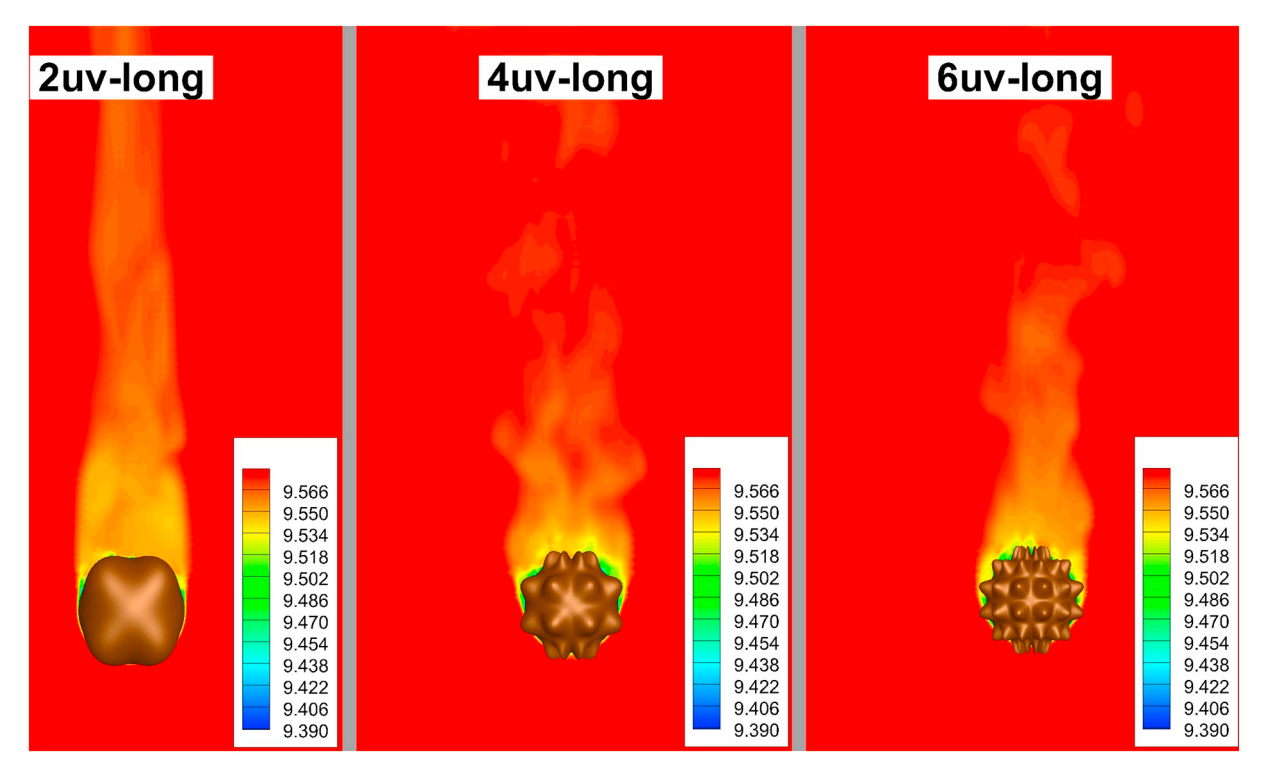


Fig. 14. Vapor density distribution in the central vertical cross-section of long-lobed hailstones of d = 5 cm at randomly chosen time frames.

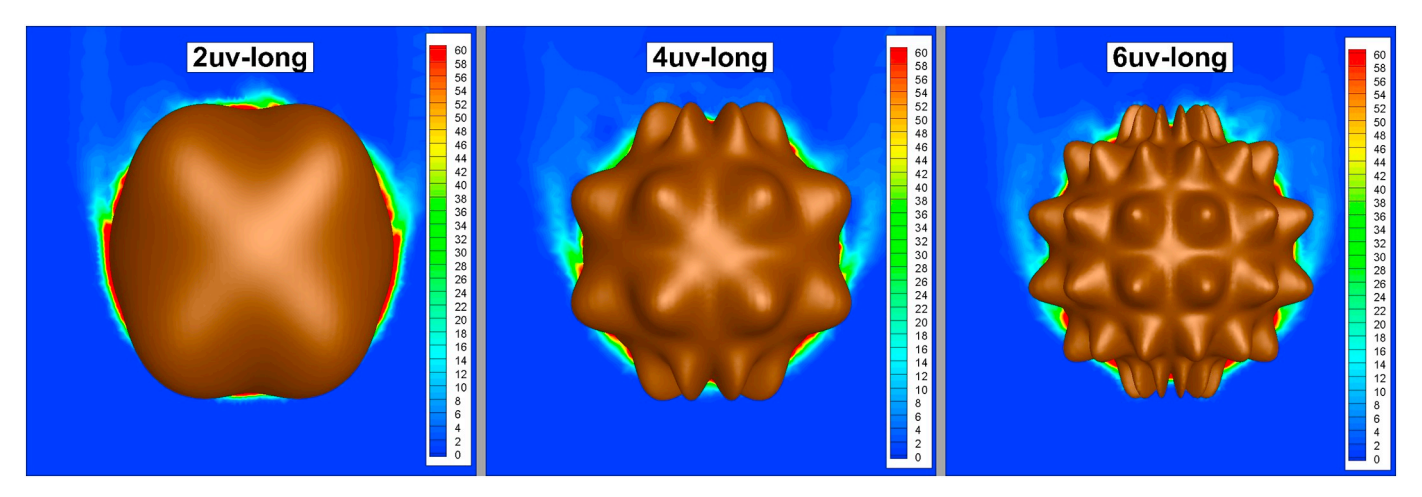


Fig. 15. Vapor density gradient distribution in the central verical cross-section of long-lobed hailstones of d = 5 cm at the time frames corresponding to that in Fig. 14.

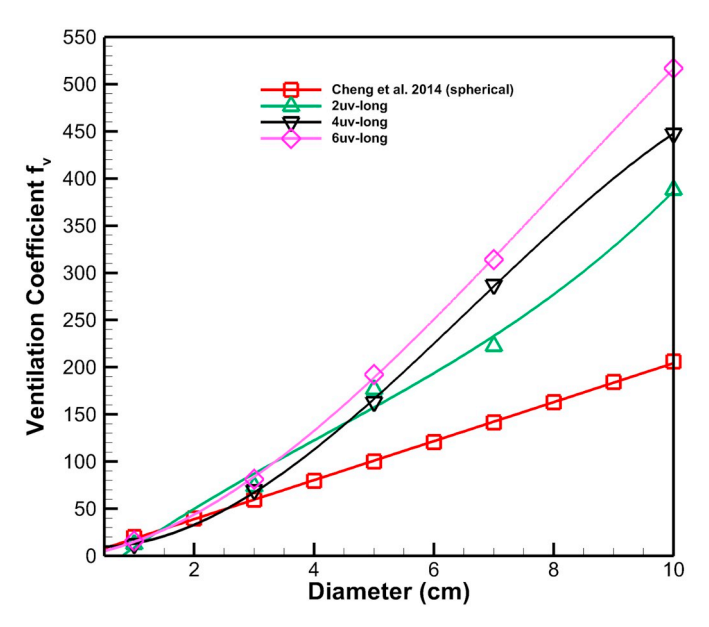


Fig. 16. Ventilation coefficient versus diameter for long lobed and spherical hailstones.

4. Summary and outlook

In the above, we presented the ventilation effect of freely falling lobed hailstones of diameter 1-10 cm by calculating their ventilation coefficients. We found that, for small lobed hailstones with diameter less than about 3 cm the ventilation effect is not much different from spherical hailstones of similar size. For larger lobed hailstones, however, the ventilation effect becomes much larger than that of similarsized spherical hailstones. The degree of ventilation enhancement generally (though not strictly) increases with the number of lobes, possibly due to the larger surface area that can absorb the vapor flux. The largest enhancement occurs in the case of 10 cm diameter 6uv-long hailstone which is about 2.5 times that of the ventilation coefficient of a 10 cm spherical hailstone. This means that the 10 cm 6uv-long hailstone can evaporate (and hence cool the air) ~2.5 times faster than a 10 cm spherical hail. This is obviously a significant difference and the ventilation enhancement by large lobed hailstones must be considered carefully when modeling severe storms that produce large hailstones.

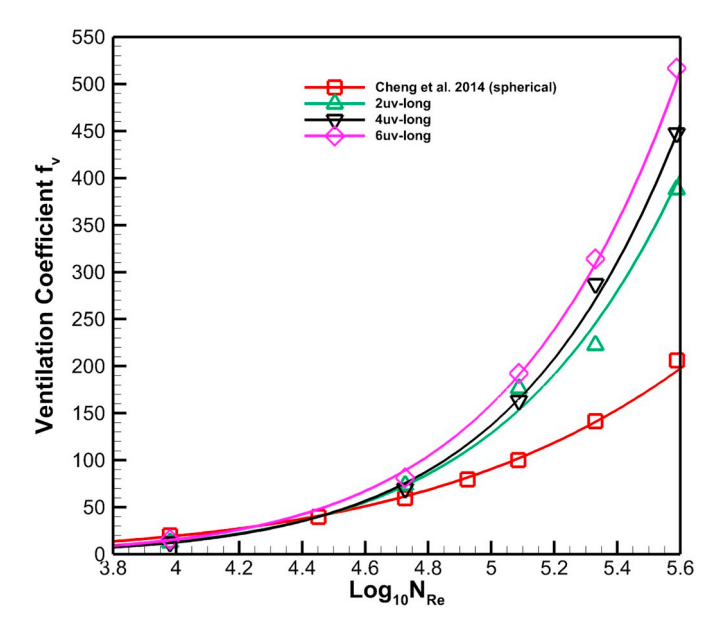


Fig. 17. Ventilation coefficient versus $\log_{10}N_{\rm Re}$ for long lobed and spherical hailstones.

Such rapid evaporative cooling due to large falling lobed hailstones in subsaturated air can be a significant factor causing strong downburst as suggested by Fujita (1985). The curve fitting equations derived from the present study can lead to better parameterizations of evaporative cooling in cloud microphysical models.

The lobed hailstones studied in this paper are all quasi-spherical as their shapes are based on adding lobes to a spherical base. Many observed large hailstones deviate significantly from spherical, are spheroidal instead, and are often with highly asymmetric irregular lobes attached to the spheroidal base (e.g., Knight and Knight, 2005). We have begun the numerical study on the fall behavior of spheroidal hailstones and will use those results to study the ventilation effects of them.

It is perhaps worthwhile to explore the implication of the present finding that the lobed hailstones have general much higher ventilation effect than spherical hailstones of similar size. We know that large hail only occurs in severe thunderstorms but so far there is no consensus of exactly how lobed hailstones form in such clouds and much less about

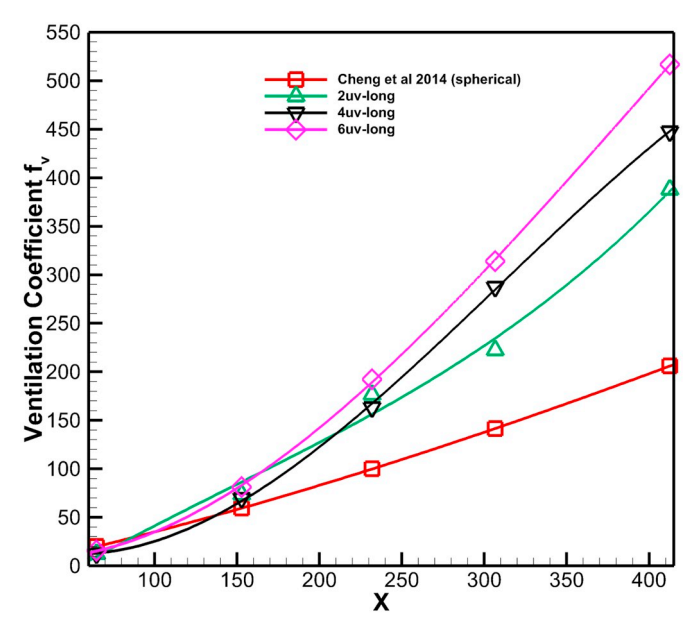


Fig. 18. Ventilation coefficient versus *X* for long lobed and spherical hailstones.

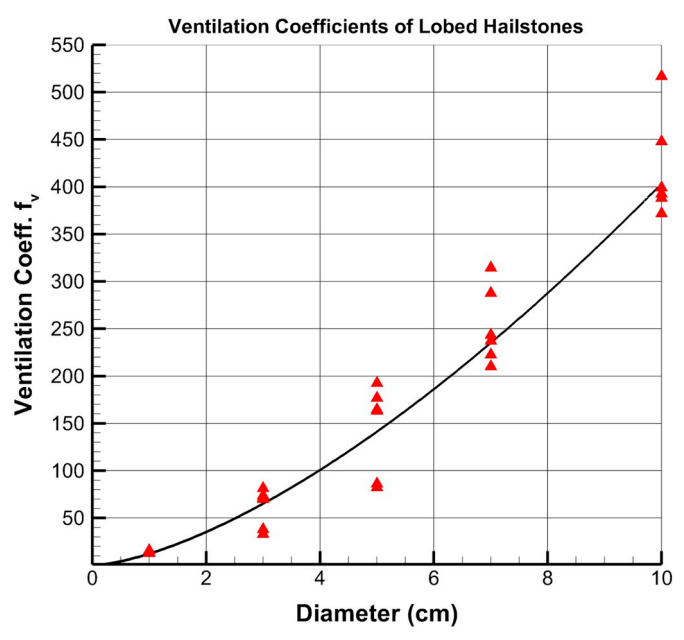


Fig. 19. Ventilation coefficient versus diameter for all lobed hailstones.

what types of thunderclouds are favorable for lobed hail production. Knight and Knight (2005) observed that the largest Aurora (Texas) hailstones, many are highly lobed and irregular, have exceptionally thick outer growth layer of clear ice and speculated that these stones must have spent a long time in warm lower part of the updraft and accumulated a significant of their large mass there. If this is indeed the case, then it implies that storms with strong low level updraft may favor the growth of large lobed hailstones which, when fall through subsaturated air, leads to strong cooling of air due to evaporative sublimation and result in strong downburst. Whether or not this is the case will need further studies.

This paper concerns with the ventilation coefficient only and hence only relevant to diffusion growth. In the growth situation, the hail size distribution is largely determined by collision growth (riming), hence the increase in ventilation coefficient probably would not affect the size distribution significantly. However, during the sublimation mode, the increased ventilation coefficient will possibly lead to narrowing the

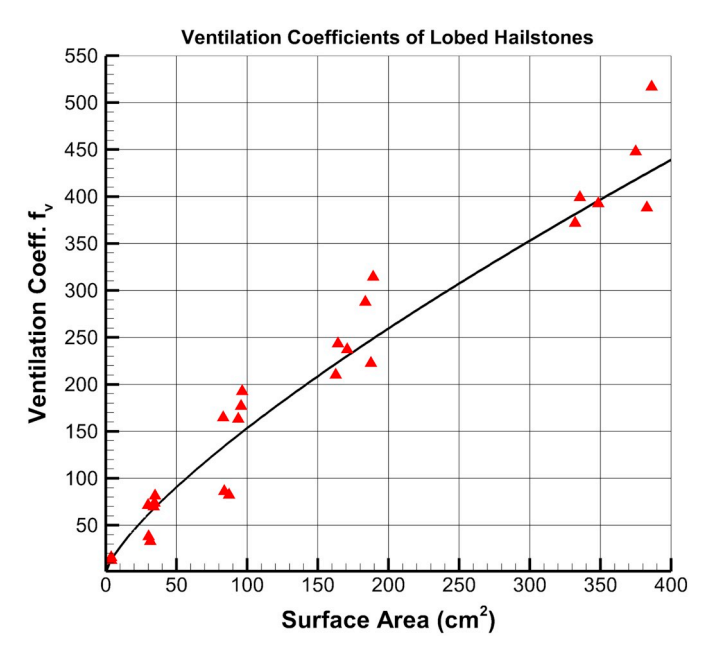


Fig. 20. Ventilation coefficient versus surface area for all lobed hailstones.

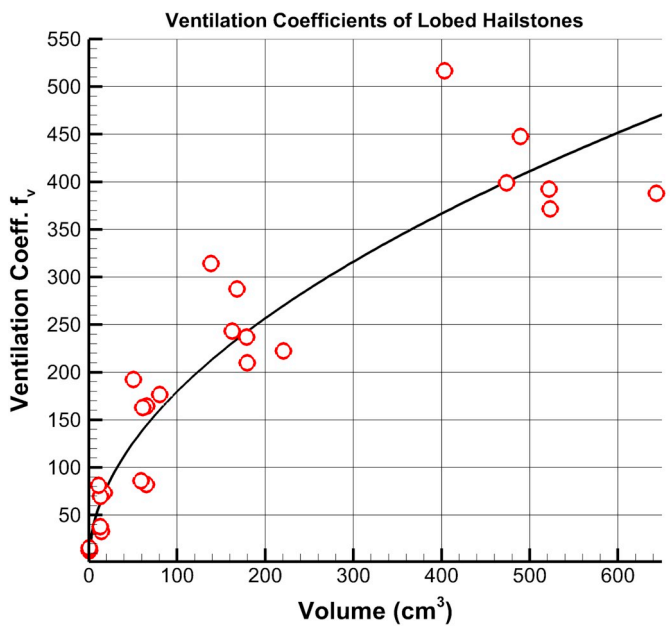


Fig. 21. Ventilation coefficient versus volume for all lobed hailstones.

spectrum as larger hailstones will sublimate faster than smaller hailstones. We will plan to investigate this point in a future project.

Declaration of competing interest

There is no conflict of interest involved in this manuscript.

Acknowledgements

We thank Dr. Jose Luis Sanchez and an anonymous reviewer for helpful comments that led to improvement of the manuscript. This study is partially supported by the US NSF grant AGS-1633921 and Academia Sinica research fund AS-TP-107-M10. Any opinions, findings and conclusions for recommendations given in this article are those of the authors and don't necessarily reflect the viewpoints of the National Science Foundation (NSF).

References

- Aguirre Varela, G.G., Castellano, N.E., Pereyra, R.G., Avila, E.E., 2003. The effect of surface lobes on heat transfer from an ice particle. Quart. J. Roy. Meteor. Soc. 129, 3425–3438
- Auer, A.H., Marwitz, J.D., Vali, G., Veal, D.L., 1971. Final Report to the National Science Foundation, Grants GA-1527 and GA-19105. University of Wyoming, Dept. Atmospheric Resources, pp. 94.
- Bailey, I.H., Macklin, W.C., 1968. The surface configuration and internal structure of artificial hailstones. Quart. J. Roy. Meteor. Soc. 94, 1–11.
- Beard, K.V., Pruppacher, H.R., 1971. A wind tunnel investigation of the rate of evaporation of small water drops falling at terminal velocity in air. J. Atmos. Sci. 28, 1455–1464
- Bilham, E.G., Relf, E.F., 1937. The dynamics of large hailstones. Quart. J. Roy. Meteor. Soc. 63, 149–162.
- Cheng, K.-Y., Wang, P.K., Wang, C.-K., 2014. A numerical study on the ventilation coefficients of falling hailstones. J. Atmos. Sci. 71, 2625–2634.
- Chou, C., Chiang, J.C.H., Lan, C.W., Chung, C.H., Liao, Y.C., Lee, C.J., 2013. Increase in the range between wet and dry season precipitation. Nat. Geosci. 6, 263–267.
- Chouippe, A., Krayer, M., Uhlmann, M., Dušek, J., Kiselev, A., Leisner, T., 2019. Heat and water vapor transfer in the wake of a falling ice sphere and its implication for secondary ice formation in clouds. New Journal Physics 21, 043043.
- Duan, Z., He, B., Duan, Y., 2015. Sphere drag and heat transfer. Sci. Rep. 5, 12304.Fujita, T.T., 1985. The Downburst Microburst and Macroburst. The University of Chicago SMRP Research Paper, Chicago (122 pp).
- Goyer, G.G., Lin, S.S., Gitlin, S.N., Plooster, M.N., 1969. On the heat transfer to ice spheres and the freezing of spongy hail. J. Atmos. Sci. 26, 319–326.
- Greenman, B.J.W., List, R., 1995. Experimental closure of the heat and mass transfer theory of spheroidal hailstones. J. Atmos. Sci. 52, 3797–3815.
- Heymsfield, A.J., Wright, R., 2014. Graupel and hail terminal velocities: does a supercritical Reynolds number apply? J. Atmos. Sci. 71, 3392–3403.
- Ji, W., Wang, P.K., 1990. Numerical simulation of three-dimensional unsteady viscous flow past fixed hexagonal ice crystals in the air — Preliminary results. Atmos. Res. 25, 539–557.
- Kinzer, G.D., Gunn, R., 1951. The evaporation, temperature and thermal relaxation-time of freely falling water drops. J. meteor. 8, 71–83.
- Knight, C.A., Knight, N.C., Dec., 2005. Very large hailstones from Aurora. Nebraska. Bull. Amer. Meteor. Soc. 1773–1781.
- List, R., 1963. General heat and mass exchange of spherical hailstones. J. Atmos. Sci. 20, 189–197
- List, R., Dussault, J.G., 1967. Quasi steady state icing and melting conditions and heat and mass transfer of spherical and spheroidal hailstones. J. Atmos. Sci. 24, 522–529.
- Lozowski, E.P., Beattie, A.G., 1979. Measurements of the kinematics of natural hailstones

- near the ground. Quart. J. Roy. Meteor. Soc. 105, 453-459.
- Macklin, W.C., 1963. Heat transfer from hailstones. Quart. J. Roy. Meteor. Soc. 89, 360–369.
- Masliyah, J.H., Epstein, N., 1970. Numerical study of steady flow past spheroids. J. Fluid Mech. 44, 493–512.
- Matson, R.J., Huggins, A.W., 1980. The direct measurement of the sizes, shapes and kinematics of falling hailstones. J. Atmos. Sci. 37, 1107–1125.
- Noh, Y.-J., Seaman, C.J., Vonder Haar, T.H., Liu, G., 2012. in situ aircraft measurements of the vertical distribution of liquid and ice water content in midlatitude mixed-phase clouds. J. Appl. Meteor. Clim. 52, 269–279.
- Pitter, R.L., Pruppacher, H.R., Hamielec, A.E., 1974. A numerical study of the effect of forced convection on mass transport from a thin oblate spheroid of ice in air. J. Atmos. Sci. 31, 1058–1066.
- Prodi, F., Levi, L., Nasello, O.B., Lubart, L., 1991. Morphology and density of ice accreted on cylindrical collectors at low values of impaction parameter. II: Rotating depositsxs. Quart. J. Roy. Meteor. Soc. 117, 783–801.
- Pruppacher, H.R., Klett, J.D., Microphysics of Clouds and Precipitation, Kluwer (1997) 954 pp.
- Rasmussen, R.M., Heymsfield, A.J., 1987. Melting and shedding of graupel and hail. part i: model physics. J. Atmos. Sci. 44, 2754–2763.
- Roos, D.S., Carte, A.E., 1973. The falling behavior of oblate and spiky hailstones. J. Rech. Atmos. 7, 39–52.
- Scheupp, P.H., List, R., 1969. Mass transfer of rough haisltone models in flows of various turbulence levels. J. Appl. Meteorol. 8, 254–263.
- Thorpe, A.D., Mason, B.J., 1966. The evaporation of ice spheres and ice crystals. Br. J. Appl. Phys. 17.
- Tlisov, M.I., Filatkin, V.N., Pilip, I.I., 1992. Heat and mass transfer of drops and growth and melting of freely floating hailstones. Atmos. Res. 28, 21–39.
- Wang, P.K., 1997. Characterization of ice crystals in clouds by simple mathematical expressions based on successive modification of simple shapes. J. Atmos. Sci. 54, 2035–2041.
- Wang, P.K., 1999. Three-dimensional representations of hexagonal ice crystals and hail particles of elliptical cross sections. J. Atmos. Sci. 56, 1089–1093.
- Wang, P.W., 2013. Physics and Dynamics of Clouds and Precipitation. Cambridge University Press.
- Wang, P.K., Chueh, C.C., Wang, C.K., 2015. A numerical study of flow fields of lobed hailstones falling in air. Atmos. Res. 160, 1–14.
- Woo, S.E., Hamielec, A.E., 1971. A numerical method of determining the rate of evaporation of small water drops falling at terminal velocity in air. J. Atmos. Sci. 28, 1449, 1454
- Zheng, G., List, R., 1994. Preliminary investigation of convective heat transfer of hailstone models. Atmos. Res. 32, 75–83.